Electronic Supplemental Information:

Quantifying the Promise of Lithium–Air Batteries for Electric Vehicles

Kevin G. Gallagher[1,2]*, Steven Goebel[1,3†], Thomas Greszler[1,3‡], Mark Mathias[1,3], Wolfgang Oelerich[1,4§], Damla Eroglu[1,2], and Venkat Srinivasan[1,5]

[1]Joint Center for Energy Storage Research.

[2]Argonne National Laboratory, Lemont, Illinois USA.

[3]General Motors, Pontiac, Michigan USA.

[4]Adam Opel AG, Ruesselsheim, Germany.

[5]Lawrence Berkeley National Laboratory, Berkeley, California USA.

*Correspondence to: kevin.gallagher@anl.gov

[†]Current address: SimuTech Group, Rochester, New York USA.

[‡]Current address: Saft America, Cockeysville, Maryland USA.

[§]Opel is a wholly owned subsidiary of General Motors.

Supplementary Materials:

Materials and Methods

Supplemental Text

Figures S1-S6

Tables S1-S5

External Databases S1-S2 (gallagherLiO2closed.xlsx and gallagherLiO2open.xlsx)

Materials and Methods:

Electrode, cell, pack, and system design. At the heart of a battery is a repeat unit that contains both the anode and cathode active materials combined with the components required to pass ionic and electronic current. An air battery further requires a means of transporting oxygen or air to and from the cell. A single layer within the cell is illustrated in the schematic in Fig. S1A. The negative electrode is composed of a thin copper foil, assumed to be 8 microns in thickness, sandwiched by lithium metal films. Stabilizing Li-metal anodes is a major concern.[1-6] Lithium-metal surface area can increase significantly with cycling due to morphological changes, a problem which occurs because of the high Li-metal reactivity. Dendrites during charging can form and cause an internal short circuit by growing through the separator. One intriguing approach under development is to protect and separate the lithium-metal electrode with a solid lithium-ion conducting ceramic.[1, 2, 7, 8] We assume the success of this development pathway for this work. The ceramic prevents electrons, electrolyte, and gaseous species at the positive electrode from crossing over to the lithium metal. The exact composition of the ceramic is not specified in this work. Rather, a large range of transport properties is assumed for the various cases examined. A barrier layer is likely necessary between the ceramic conductor and the

lithium metal to prevent the reduction and decomposition of the solid electrolyte. Reports have shown that films such as Li_3N may be sufficient as barriers.[8] While we have not explicitly accounted for such a layer, we have assumed a 50% excess of lithium is necessary to meet battery life goals. Past commercialization attempts have required upward of 300% excess lithium.[4, 6]

A long-lived seal between the ceramic and copper foil will be difficult to engineer while minimizing the volume impact on the cell. The foil and ceramic are 8 and 20 microns in thickness while the anode volume change may be on the order of 100 microns. A large development effort will be necessary to achieve simple manufacture and the mechanical integrity and hermetic properties necessary over the 1000 cycles expected over the battery life. Additionally, the seal material needs to be chemically resistant to the electrolyte solvent. We have envisioned a number of possible sealing approaches, all of which include having the ceramic and foil extend beyond the active area by a few millimeters in length. In one potential approach, the perimeter of the foil would be coated with an adhesive, and then the ceramic would be pressed against the foil. In other words, the perimeter of the ceramic would be flexed and pressed against the adhesive to seal. Figure S1 does not show the entire seal, as the dimensions are much larger than the thickness of a single layer.

The positive electrode is porous and includes an electron-conducting carbon-like phase, lithium-ion conducting electrolyte phase, and gas phase. We have assumed that a range of surface energies and pore sizes exist in the carbon-like matrix to maintain continuous electrolyte and gas percolation networks. This carbon-like matrix is taken to have similar, but more advanced, physical properties of the various carbon papers and felt materials in commercial production today. Carbon black oxidizes in Li/O_2 cells and will likely need surface modification for use or be replaced with a more stable electron conductor. [9-11] The precipitation of the product phase, Li_2O_2, is envisioned to fill the void space, reducing the porosity available for gas diffusion, but not to impede the transport of ions and electrons. We have assumed passivation from the insulating product has been overcome through control of the combined charge and mass transport processes occurring within the electrode. Additionally, we assume that the electrolyte and electrode has reached the level of stability needed to enable the resulting battery to meet life-time targets for automotive applications.

Finally, the positive electrode current collector is a corrugated aluminum metal sheet that also serves as a flow field to transport oxygen to and from the electrode. The flow field is an efficient design to minimize the parasitic volume required to achieve reasonable pressure drops. The thickness of the aluminum necessary to enable this design is uncertain. We have studied aluminum thicknesses up to 100 microns and found significant mass and cost penalties. However, this sensitivity is small compared to that of the gas utilization components analyzed in detail below. An alternative electrode design variation might use porous media rather than a channel-based flow field. Removing the corrugation demand of the aluminum foil simplifies the design by using the positive electrode for the electrochemical reaction and also as the means of transporting oxygen across the cell area. The porous media approach results in an unacceptably large pressure drop when flowing air is used, but appears suitable for operation with pure oxygen. More details on the sizing of the flow channels can be found below.

The cells are composed of multiple stacked bilayers whose current collectors are welded together at the tabs to produce a single cell voltage unit, as shown in Fig. S1B. The number of bilayers, electrode loading values, and flow field dimensions are all sized to the meet the

required battery performance. The area of a single layer was designed to be near dimensions suited for transportation applications, 250-500 cm^2. The total number of bilayers is set by the cell capacity, the electrode thickness, and the area required for the target power and energy.

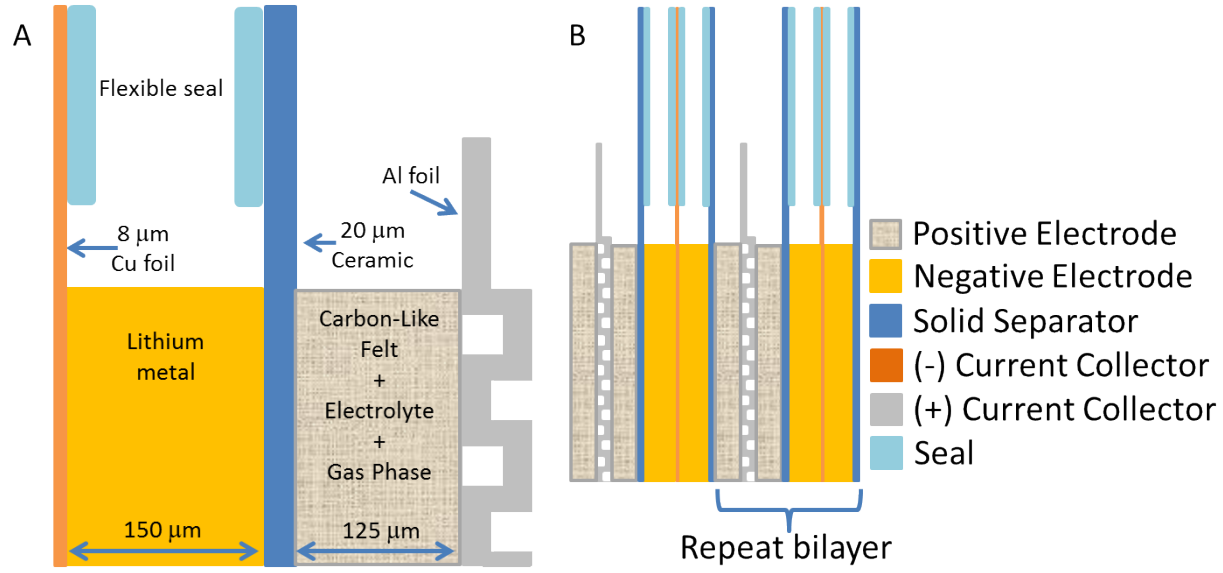

Fig. S1. (A) Schematic of a single layer within a Li/O_2 cell, with example dimensions of various components. (B) Schematic of multiple layers in a bilayer arrangement. Seal of ceramic to copper foil is not shown due to the longer length scale compared to the thickness of the layer.

The completed cell (i.e., stack of bilayers) with welded terminals is wrapped with a tri-layer material, similar to that used in Li-ion pouch cells, to create a cohesive unit, provide a level of structural stability, and hinder any electrolyte transport pathways between cells. The material is composed of 100-micron aluminum foil sandwiched between a polyethylene terephthalate and an inner layer of polypropylene. The top and bottom of the cell are left open to allow gas access to the flow channels. These cells are then arranged into modules to form a building block for the battery. The module structure provides rigidity as well as houses the state-of-charge controllers for each series-connected cell group.

Both the cells and modules must be engineered to handle the large volume changes that take place within each layer. The various electrical, and perhaps heat transfer fluid, connections made within a module must be adaptable to the large volume change, or alternatively, a fixed volume unit may be maintained with the use of springs or additional components. In practice, one might expect the addition of 100% of the volume change, *ca.* 10-20% of the pack volume, to be added within the battery in the form of springs or foams to accommodate the full change in volume that occurs on discharge. We have not included any allotment for these components.

The module as well as the pack enclosure must make allowances for introducing oxygen or air into the cells. The pack enclosure will vary depending on if one attempts to design and manufacture a closed or open system. A closed system is one in which the oxygen is stored in a pressurized vessel, and thus, normal constituents from the outside air are not a concern (water, carbon dioxide, etc). The open system must compress the air, provide several operations to

prepare the air flow to enter the cell stack, and treat the effluent before releasing it back to the surrounding atmosphere. In the closed system, the tank serves as both the pressure vessel to contain the oxygen and the housing that provides structural support to the battery modules. The resulting rigid structure integrates the electrochemical storage system into the structural frame of the vehicle. The open system is envisioned to have battery packaging similar to commercial Li-ion transportation packs, with some allowances for the convection of air through the modules and cells. Figure S2 illustrates how the cells are situated within the enclosure in the two approaches.

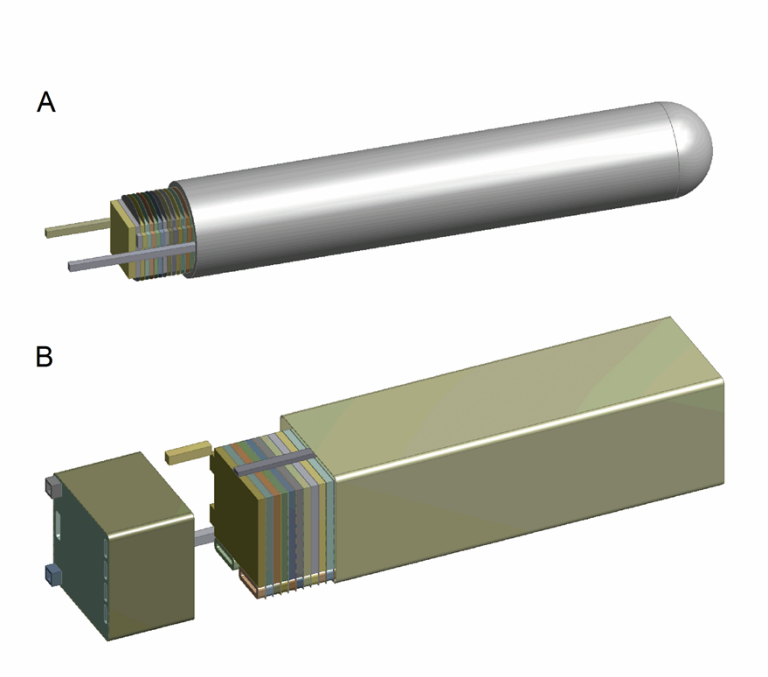

Fig. S2. Illustration of the enclosures for the closed (A) and open (B) systems.

The thermal management approach for the two architectures will differ, as the closed system is limited by the number and type of connections that feed through the pressure vessel. For example, passing a cooling fluid into the closed system would require excessively heavy feed-throughs to handle the large pressure difference. For the closed system, aluminum heat sinks are used to transfer thermal energy to and from the cells via conduction. The outer vessel walls are jacketed with a 0.5-mm flow passageway in which a 50/50 mixture of ethylene glycol and water solution is flowed. This approach limits the heat rejection rate and motivates the use of smaller area cells to reduce temperature non-uniformities. Moreover, the rate at which the battery is discharged could be limited, although the applications considered here will not be affected. The open architecture utilizes the same thermal management approach used for other advanced batteries considered, in which a heat transfer fluid taken to be 50/50 ethylene glycol-water solution is forced through a manifold below the cell stack and up in-between every other cell via a double-walled cooling plate containing flow channels. Lightweight, high-efficiency thermal insulation (10 mm thick) is wrapped around the outside of each battery pack to slow the thermal interactions of the battery under ambient conditions.

Model and calculation methodology.

Electrochemical Performance Model

The current-potential behavior is based on a system of algebraic equations that account for the charge transfer and ohmic resistances within the electrochemical cell. Materials-level values are provided as a guide to researchers, thus enabling the benchmarking of current technology and the establishment of performance goals for future prototypes. The current collection resistances are addressed in the manner described elsewhere.[12] Additionally, ohmic losses from electron transport through lithium metal are neglected due to the high conductivity. The equations used are described below as if the cell is being discharged (i.e., Li moving left to right in Fig. S1A).

The transfer current, i_n, of lithium from the metal surface into the solid ceramic electrolyte is treated with the Butler-Volmer equation, Eq. S1. Here, i_0 is the exchange current, α_a and α_c are the transfer coefficients, and η is the surface overpotential. Concentration overpotentials are neglected in this treatment. Additional parameters are Faraday's constant, F, the universal gas constant, R, and the temperature, T. The lithium metal and ceramic interfaces are taken to be planar; thus, the current density, I, is equivalent to the transfer current.

$$i_n = i_0\left[\exp\left(\frac{\alpha_a F}{RT}\eta\right) - \exp\left(\frac{\alpha_c F}{RT}\eta\right)\right] \tag{S1}$$

Ohmic losses from the transport of lithium ions within the ceramic solid electrolyte are quantified with Ohm's law, Eq. S2. Here, κ_{solid} is the ionic conductivity, and $\Delta\Phi_2$ is the potential drop across the thickness of the ceramic. The transport of lithium ions across the ceramic interface into the electrolyte phase of the positive electrode is treated with Eq. S1.

$$I = -\kappa_{solid}\Delta\Phi_2 \tag{S2}$$

Determination of the overpotential associated with the positive electrode is more complex due to current distribution within the porous electrode. Newman and Tobias provided analytical expressions that account for changes in current distribution within the porosity of the electrode for approximations that neglect concentration gradients and any role of the precipitant product phase.[13] Moreover, a single analytical expression that covers the entire current-potential behavior of the Butler-Volmer equation is not available. The correct expression must be selected on the basis of the suitability of a linear or Tafel approximation. The governing equations using porous electrode theory for the positive electrode are detailed in Eqs. S3-S6. Here, $\mathbf{i}_1$ and $\mathbf{i}_2$ are the matrix and electrolyte phase superficial current densities, respectively. Likewise, Φ_1 and Φ_2 are the matrix and electrolyte potentials. The electrolyte, κ, and matrix, σ, phase conductivities are corrected for the porosity and tortuosity by multiplying their bulk values by the volume fraction to the 1.5 power. The difference between the matrix and electrolyte potentials is the surface overpotential. The specific interfacial area is represented by a. The transfer current is described by an approximation of the Butler-Volmer equation, Eq. S1, in either the linear form or Tafel expression. Conservation of charge dictates that the divergence of the total current is zero, Eq. S6.

$$\mathbf{i}_1 = -\sigma\nabla\Phi_1 \tag{S3}$$

$$\mathbf{i}_2 = -\kappa \nabla \Phi_2 \quad \text{(S4)}$$

$$\nabla \cdot \mathbf{i}_2 = a i_n \quad \text{(S5)}$$

$$\nabla \cdot \mathbf{i}_1 + \nabla \cdot \mathbf{i}_2 = 0 \quad \text{(S6)}$$

The boundary conditions specify zero current for the matrix at the electrode-to-ceramic boundary and also for the electrolyte phase at the electrode to current collector boundary. The electrolyte current is equivalent to $-I$, and the electrolyte potential is arbitrarily set to zero at the electrode-to-ceramic boundary. The solutions to these equations may be found in Newman and Tobias's work.[13] The model used here selects the correct approximation to the Butler-Volmer equation depending on the value of the current density and kinetic parameters.

The parameters used within the model equations determined the overall performance of the battery and, thus, the projected energy density and cost. We considered a broad range of values so as to map the entire design space, Table S1. The conductivities of the electrolyte and electronically conductive matrix phase were taken to be those in existing Li-ion systems. The more optimistic cases used charge transfer values more favorable than those reported in the literature. Using this approach allows one to consider what would be necessary at the materials level to achieve an enhanced performance at the systems level. The parameters were varied in a manner so that all improve together, and single-value sensitivities were not studied. We note that a different combination of material values could give rise to the same design as the combinations shown below. In Table S1, the lower and upper bound are presented for the model parameters in each region of the layer. The actual simulations used multiple values between the upper and lower bound to produce a smooth function. Some values are correlated and then best considered together when defining performance objectives. For instance, the product of the exchange current and specific interfacial area, $a \cdot i_0$, is inseparable in the polarization calculations. The conductivity and thickness of the ceramic solid electrolyte can be considered in a similar manner, although the overall mass and dimensions of the ceramic plate do affect the mass, volume, and cost of the pack.

Table S1. Parameter values for each charge transfer step within the electrochemical cell.

Charge transfer step	Parameter[a,b]	Value	Reference
lithium/ceramic	i_0 (A/cm^2)	$10^{-4} - 10^{-3}$	14-16
ceramic	κ (S/cm)	$10^{-4} - 10^{-2}$	17-19
ceramic/electrolyte	i_0 (A/cm^2)	$10^{-4} - 10^{-3}$	16
lithium-oxygen reaction[c]	i_0 (A/cm^2)	$10^{-5} - 10^{-3}$	20

[a] All parameters given at 30 °C.

[b] Li^+ charge transfer assumes α_a, $\alpha_c = 0.5$.

[c] Specific interfacial area, a = 5,000 cm^{-1}, used with the exchange current assumes an active specific surface area of 10 m^2/g, which equates to a loading of 0.5 mg/cm^2 for a 100-μm thick electrode.

The electrochemical inter-conversion of Li^+-O_2 and Li_2O_2 appears to leave the oxygen-oxygen bond intact and thus is more kinetically favored over the full four-electron pathway

typically sought in the oxygen electrochemistry in aqueous electrolytes. The exchange current associated with the electrochemical inter-conversion thus uses more favorable values, Table S1. The exchange current will also be a function of oxygen partial pressure and electrode material, though some conflicting data exist in relation to this dependency [21-24]. We assume no direct relationship between oxygen partial pressure and the exchange current in this model. The exchange current values cover a broad enough performance range to capture advantages gained from higher oxygen partial pressures.

Oxygen Delivery within the Cell

Uniform oxygen partial pressure must be present within each cell and across the full positive electrode layer area to achieve optimal performance, life, and utilization. Flow passages with the least flow resistivity will allow the most shallow flow field depth and, therefore, smallest battery size. It is also of interest to minimize cost by simple and continuous fabrication. In these regards, straight flow passages formed by corrugation of the positive current collector are a very favorable option, as illustrated in Fig. S1. The straight-through channels reduce the flow path length, and an open channel is non-tortuous and has the largest possible open area (compared to porous material) for the lowest pressure drop or smallest flow field thickness. Although the formed channel configuration is favorable (from a size and cost perspective), it may not be feasible. Of particular concern is the forming of the small channels that are desired (typically 20-60 microns deep for the conditions considered), that the thin foil retains this formed shape when compressed, and that the electrode material remains intact and does not creep into the channels. The baseline case of 20-micron thick aluminum was considered, as it sets the lower limit of what would be possible. For a square-channel-type flow field used in the open-architecture system, the laminar pressure drop, Δp_{ch}, was determined as shown in Fig. 1, where μ is the viscosity, l is the flow path length, $\dot{Q}$ is the volumetric flow, D_{ch} is the channel hydraulic diameter, and S is the cross-sectional flow area. For the channel configuration, the channel width was taken to be the same as the channel depth.

An alternative approach is to use a porous material for the flow field. Due to significant pressure drop, this approach likely requires a pure oxygen environment so that nitrogen does not need to be moved through the flow area. A new challenge in this approach is that the pores of the flow field could become filled with liquid electrolyte; thus, the material system will require tailored surface energy and pore sizes of the electrode with respect to the porous flow field. The pressure drop, Δp_{por}, for a porous material type flow field is also shown in Fig. 1, where the K is the permeability, and S is the superficial flow area. For the closed-architecture Li/O_2 system, where the electrode would also be used as the porous flow field, the Carman-Kozeny equation was used to calculate the permeability. We assumed closed packed spheres and void porosity at 15% state of charge. The permeability was calculated to be 1.4×10^{-13} m^2, resulting in only 2-kPa pressure drop within the electrode for the closed system utilizing pure oxygen. This small pressure drop is likely to cause only minimal performance variation across the cell. However, using porous media, with a permeability of 1×10^{-12} m^2 based on existing flow battery materials, to replace the flow channels in the open-architecture Li/O_2 system would result in unacceptably large flow passage thickness to maintain the 30-kPa target pressure drop (e.g., 300 compared to 30 microns for formed channels). The difference between the closed and open system is the requirement of transporting the nitrogen along with the oxygen over the longer flow path. Additionally, the closed system utilizes pure oxygen that may be transported from both sides of the cell, while the open system requires an entrance and exit for the flowing air.

Manifolds are also needed to deliver air from the system air supply to each of the cells. The pressure drop in the flow fields within the cells should be an order of magnitude more than the dynamic pressure in the manifold to ensure uniform distribution across the entire string of cells. The open space within a battery enclosure (necessary to accommodate cell voltage tabs and coolant headers, for example) is calculated to be adequate to provide air flow to the cells, provided the foils and terminals are constructed in a way to ensure access to the flow fields or porous media. Based on this calculation, the favorable assumption was made that an air battery would not require any additional size, mass, or cost to provide the air manifolds as this function could be provided by the pack enclosure, which is needed for conventional battery packs already.

Sizing and costing of open-system gas utilization components

Many of the components exist today that are needed in the open-system architecture, such as compressors, membrane units, and pressure-swing adsorption beds. However, the existing components are not designed for the size and cost requirements of a Li/O_2 energy-storage system for automotive applications. This situation is one that commercial product developers face whenever developing a new technology. The approach to project the high-volume cost and size of the component optimized for automotive applications is not an exact science. Engineering analysis and past experience are invaluable guides to scaling the values of existing technologies to those that might be reached under an optimistic development effort. Additional input may be obtained from considering high volume production units that have some similarity, such as supercharger compressors and electric motors for automotive applications. Our one departure from standard practice is to take the most optimistic assessment wherever possible to avoid the projection of a false negative result. In some circumstances, this approach leads us to make estimates that are an order of magnitude lower in cost than prices quoted by current suppliers. To aid in this analysis, we commissioned an expert analysis and sizing from InnoSepra (Middlesex, New Jersey) for a dual-bed pressure-swing adsorption unit operating 0.7 MPa that would meet automotive specifications.

A listing of the components for a range of possible system configurations is given in Table S2. Thermal management is required with most of the components shown. The compressor is necessary to pressurize and move air through the various portions of the battery. We have analyzed a moderate pressure approach using 0.3 MPa and a high pressure approach using 0.7 MPa. All pressure values in this manuscript are absolute rather than gauge values. Increasing operating pressure will reduce the size of the pressure-swing adsorption beds but result in a larger and more costly compressor, motor, and heat exchanger. Increasing pressure also requires a greater parasitic power draw from the battery and, thus, a larger battery. A displacement-type compressor is needed to provide high pressure at low flow rates and low power operation. Additionally, oil-free operation is required to avoid oil contamination of the pressure-swing adsorption unit and the Li/O_2 battery. A single-stage rotary screw compressor can provide up to 10:1 pressure ratio, but only in an oiled version (for cooling and sealing). For an oil-less version, two stages would be needed to achieve the 0.7 MPa desirable for the pressure-swing adsorption unit. The two-stage compressor and motor size, mass, and cost would approximately double over the single-stage 0.3 MPa estimate, as the components would double and require higher power operation.

We selected a pressure-swing adsorption separation unit that utilizes dual beds to provide continuous adsorption and regeneration and would provide comparable powertrain operation to that currently expected by consumers in automotive applications. The alternative of temperature-

swing adsorption has an unfavorable lag time associated with cooling the thermal mass of the separation unit to optimal adsorption temperatures before driving is possible. The exact specifications for water and carbon dioxide removal in the separation unit are still uncertain; however, estimations of the potentially irreversible consumption of lithium led to a target of 1 ppmv for both carbon dioxide and water in the air stream that enters the electrodes. Estimations for 10 ppmv resulted in only slightly smaller separation units. The 0.3 MPa pressure-swing adsorption unit was estimated from the rigorously sized 0.7 MPa unit via residence time.

The use of an electrolyte solution with finite vapor pressure will require components to add solvent into the air stream before entering the cells, as well as to remove the solvent before the air exits into the surrounding environment. The sizing of these components will directly depend on the vapor pressure of the solvent. We have assumed properties similar to dimethyl sulfoxide as a guide (e.g., vapor pressure of 0.2 kPa at 40 °C, which equates to an annual loss of 10 kg, which is all of the electrolyte solvent if not mitigated). Higher vapor pressure solvents will result in larger system size. The solvent volume is sized for annual driving habits to prevent emission of solvent in the exhaust or dry out of the battery. An alternative approach might utilize a membrane unit to transfer a portion of the solvent from the exit stream to the entry, thereby reducing solvent consumption; however, our estimations found similar system size and cost.

Table S2. Volume, mass, and cost for components that could be used in the open-system gas utilization architecture.

Component	Volume (L)	Mass (kg)	Cost ($)
Air filter	4	2	15
Single-stage 0.3 MPa screw compressor, motor, cooling	15	18	650
Two-stage 0.7 MPa screw compressor, motors, cooling	30	36	1300
0.3 MPa pressure-swing adsorption system	38	38	600
0.7 MPa pressure-swing adsorption system	25	25	500
Solvent addition (100% vapor loss)	14	12	70
Solvent capture (100% vapor loss)	15	13	100
Fan for oxygen dilution to atmosphere	3	2	10

Pressure vessel

The pressure vessel for the Li/O_2 closed architecture assumed the use of aluminum alloy 6061 (Al-alloy) to contain the 15-20 MPa of pressure at full charge. The cylindrical tank capped with hemispherical ends would be flanged or welded to allow for the insertion of the stack within the tank. The wall thickness was calculated from the overpressure and the tensile strength, assuming a design factor of 2.25 to prevent vessel rupture, Eq. 6 in Vorhees et al.[25] The volume of hemispherical ends was taken to be equivalent to the battery solid material not explicitly accounted for in the model, and thus, this space was not used for holding gaseous oxygen. The unspecified solid material contributions would include any structural components to hold the stack within the tank, porous media to mediate solvent vapor condensation, and structural support for the terminal feed-through. A parallel-connected stack arrangement is used. A single tank would require diameters larger than feasible for heat transfer purposes or tanks longer than acceptable for the vehicle frame. The physical properties and cost for the Al-alloy, steel, Ti-alloy, and carbon-fiber composite are detailed in Table S3. The costs were derived from engineering estimates based on automotive experience with hydrogen tanks and reflect both a raw material and forming contribution to the end cost. The tensile strength for the carbon fiber

composite was reduced from 2050 MPa by a factor of one-third to match the design wall thickness calculated using a proprietary tank-sizing model employed at General Motors. The composite nature and irregular winding of carbon fiber lead to a reduction in effective tensile strength in application of these pressure vessels.

Table S3. Tank wall material properties used to design pressure vessel for Li/O_2 closed system

Tank Wall Material Properties	Steel	Al Alloy	Ti Alloy	Carbon Fiber
Tensile Strength (MPa)	460	300	800	1367
Density (kg/L)	8.0	2.7	4.5	1.9
Cost ($/kg)	2.5	5	26	65

Materials considered within the cell

In addition to Li/O_2 energy-storage systems, this study considers several Li-ion and advanced Li-ion materials to provide a context for the Li/O_2 estimates.[26] The active materials considered in this study are detailed in Table 1 with their pertinent characteristics. The cathode materials include two intercalation hosts of Li-ion layered transition metal oxide. The NMC333 material has a stoichiometry near $Li_{1.05}(Ni_{1/3}Mn_{1/3}Co_{1/3})_{0.95}O_2$ and is currently used in various consumer electronics and automotive Li-ion battery applications with estimated price of $30/kg. The lithium- and manganese-rich variation, LMRNMC, has a less certain stoichiometry as development is still progressing. $Li_{1.13}Ni_{0.27}Mn_{0.54}Co_{0.06}O_2$ can be considered one example of a potential stoichiometry projected to be near $20/kg due to lower cobalt and nickel content. The anode materials other than lithium metal include surface-modified graphite, a standard commercially available product near $20/kg, and a composite silicon alloy material estimated at $25/kg. The silicon composite is of unknown stoichiometry as it is also under development. The composite may include the addition of graphitic additives or transition metals alloyed with silicon. The impedance behavior of NMC333/Gr in the BatPaC model was used for all the Li-ion related chemistries studied. The range of calculated systems-level values was estimated by examining various electrode thickness limitations from 70 to 200 microns.

The oxygen electrode in the Li/O_2 cells used 9% carbon and anticipated 88% Li_2O_2 on a solids mass basis (i.e., no electrolyte). The binder makes up the remaining 3%. For the air battery community, the specific capacity of the discharge product is often reported per gram of carbon in the electrode. Our optimistic assumptions result in a mass-specific capacity of 11,088 mAh/g-carbon for the Li_2O_2 discharge product. We assumed 25% as the default electrolyte volume fraction for all porous electrodes, including the composite silicon alloy in the lithiated state. The graphite and composite silicon alloy cells used a negative-to-positive capacity ratio of 1.1 while the lithium metal cells were designed with a ratio of 1.5. The solid ceramic used had an assumed thickness of 20 microns and density of 4 g/cm^3. The cost was taken to be $25/kg, consistent with other high-volume manufactured metal oxides, which equates to $2/m^2$. Since this material is of unknown chemistry and manufacturing process, the uncertainty associated with this value is significant. For comparison, the olefin-based porous separators currently used in Li-ion batteries are generally considered to reach costs near $2/m^2$ and less under high volume assumptions. The novel carbon-like felt structure for the oxygen electrode was assumed to be $50/kg based on a quotation from a manufacturer of advanced carbon felts. Since our optimistic analysis uses only 8% volume fraction carbon in the electrode, this equates to $0.80/m^2$ for a 100-micron thick

electrode. The felt thus contributes a negligible quantity to the total cost of the Li/O_2 battery. Thin carbon felts are currently purchased at much higher prices for fuel cell and redox flow battery prototypes, but will likely decrease in cost with increased volume and competition. The cost assumptions for the ceramic conductor and porous carbon electrode highlight the level of optimism used in this analysis in projecting the future cost structure of Li/O_2 energy-storage systems.

Manufacturing cost

The calculated cost values are the summation of a calculated price to the original equipment manufacturer, with the addition of pack integration components assumed to be completed by the automaker. Manufacturing production volumes were assumed to be 100,000 batteries per year. For the high-energy-content electric vehicles evaluated, this production volume results in favorable economies of scale, reducing the contribution of manufacturing cost to the total price. The cost calculations assume a manufacturing facility similar to one for Li-ion batteries, except that negative electrode processing, here considered as calendering and slitting, was included within the dry room due to the reactivity of Li-metal electrodes. These additional depreciation and utility costs are more than offset by the removal of the negative electrode suspension preparation and coatings processes. The uncertainty ranges included in the cost for energy include contributions from design variations, as well as large variations in the purchase price for the top material contributions. The calculated performance and cost estimates assume that a large investment in materials, engineering, and manufacturing research and development has resulted in the removal of bottlenecks and unnecessary, over-engineered components in the battery pack. Thus, the projected values will be difficult to achieve if these investments are not made, high volumes are not reached, and a competitive, market-driven electric vehicle market does not exist. The greatest value from these results is in the comparison of the projected range of outcomes for competing technologies against each other, rather than an evaluation of the absolute values estimated.

Supplemental Text:

Utilizing oxygen in the Li/O_2 battery. The open-system air utilization architecture is a complex collection of components with interdependencies that affect the total size, mass, and cost of the complete energy-storage system. The open architecture selected for this systems-level analysis is illustrated in Fig. 2A. As shown in Table S2, the size of the compressor is inversely proportional to the size of the pressure-swing adsorption system. We compared the complete energy-storage system in Table S4 to determine whether the moderate 0.3 MPa or higher 0.7 MPa approach is the most fruitful. Note that the stack was designed to operate at 0.3 MPa regardless of selected compressor to avoid the heavy structural components necessary to withstand the large differential pressure. The 0.7 MPa system requires significant parasitic power and energy to operate at this pressure, which results in a larger and more expensive battery pack. We selected the moderate pressure (0.3 MPa) approach for the open architecture as it results in the most favorable cost, volume, and mass for the complete energy-storage system. The estimated performance of the pressure-swing adsorption system used in this study requires optimistic assumptions regarding the development and use of advanced adsorbents that may be constructed

into a solid monolith for the automotive application. The regeneration/adsorption switching time for the beds was calculated to be 1.25 minutes.

Table S4. Characteristics for open-system gas utilization based on compressor pressure, including parasitic power and energy demand from the system (neglecting cooling energy). Systems-level values provide a comparison of the total penalties from the components and additional energy requirements.

Metric	0.3 MPa	0.7 MPa
Maximum parasitic compressor power (kW)	7.7	17.4
Parasitic compressor energy for C/5 discharge (kWh)	8.6	19.0
Gas utilization system cost ($)	1,445	1,995
Gas utilization system volume (L)	89	91
Gas utilization system mass (kg)	85	90
Total energy-storage system cost, no catalyst ($)	9,414	10,458
Total energy-storage system volume (L)	244	258
Total energy-storage system mass (kg)	260	279

The values in Table S4 do not include additional volumetric penalties for the necessary ducting and the more significant loss of volume (e.g., commonly double the volume) from providing access to all of these components for the routine service. Based on the previous experience and expertise of the authors, the total system volume of an installed unit is likely to be substantially greater than our best-case predictions. Upon consideration of the challenges presented by the open system, the engineering investment necessary to approach the projected values, and significant risk of falling short of a functional system, the closed system is a potentially attractive alternative.

We selected an Al alloy for the pressure vessel material based on a comparison (Fig. S3A) of tank cost, volume, and mass for four materials: steel, Al alloy, Ti alloy, and carbon fiber. The Al alloy is only slightly more expensive than the steel tank, but offers significantly lower mass. The Ti alloy and carbon fiber materials result in significantly lighter tanks but at great expense. The carbon fiber tank has two important limitations that should be considered, particularly when valuing the dramatically small estimated mass. First, the cell stack must be inserted and sealed within the pressure vessel. Metal tanks may use a flanged opening that is later sealed or perhaps welded with or without a flange. Neither flanging nor welding is an option for a carbon fiber tank. Carbon fiber tank fabrication involves high temperatures to set the composite, preventing tank manufacture around the preassembled cell stack. The second limitation is that heat transfer during battery operation must be facile through the tank material to enable effective thermal management of the battery. The carbon fiber composite has unacceptably low thermal conductivity values (e.g., 0.5 W/m·K vs. 200 W/m·K for aluminum). A path to overcome these two challenges has not been identified for the carbon fiber composite.

The design of the closed system used prismatic cells within a cylindrical pressure vessel. One might wonder if smaller system volumes could be achieved by designing circular cells to minimize void space that occurs from having a square object within a round hole. Ignoring the manufacturer challenges of fabricating high-yield circular cells and maintaining the same solid mass volume, a parametric analysis of the tank diameter in Fig. S3B demonstrates no benefit in

cost and minimal benefit in volume from going to smaller tank diameters considering the baseline design is 25 cm. Some amount of void space is necessary to contain the pressurized oxygen reactant. Shrinking the inner tank diameter increases the tank pressure, thereby increasing the wall thickness (i.e., mass) necessary to contain the pressure.

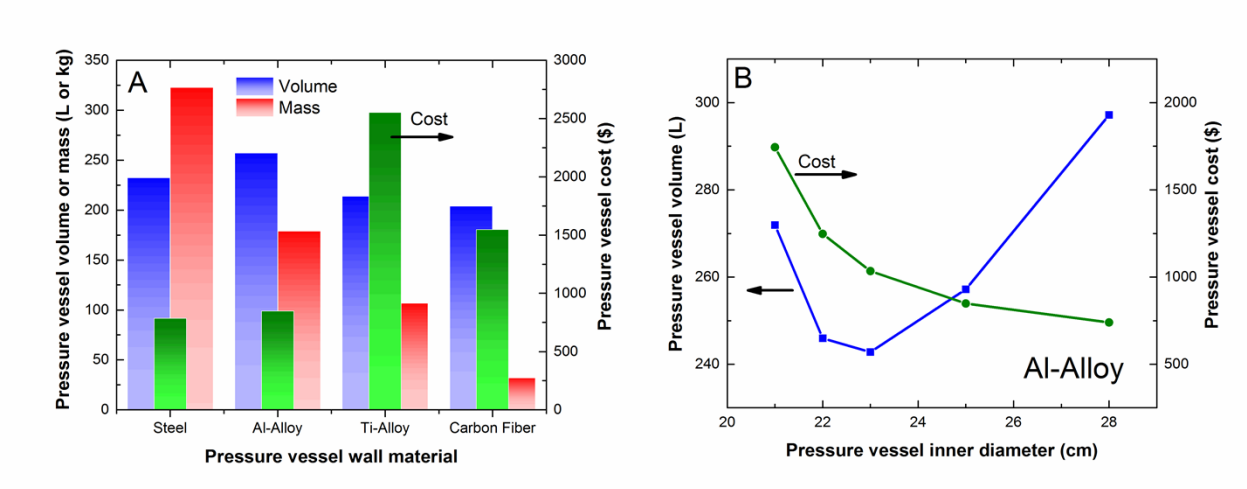

Fig. S3. (A) Analysis of pressure vessel material. (B) Sensitivity of Al-alloy pressure vessel inner diameter (baseline is 25 cm) to vessel volume and cost used in a Li/O_2 closed system with 100 kWh of useable energy.

Systems-Level Specific Energy, Energy Density, and Cost for Energy. The estimated systems-level specific energy and energy density shown in the main text in Fig. 3 are a collection of point estimates based upon various materials-level performance values and cell configurations. The cell design variations result from considering a range of maximum cell capacities (i.e., parallel-connected cells). The maximum designed cell capacity may be limited due to poor aging or abuse characteristics. The estimates of specific energy and energy density do not include uncertainty in the system components that are examined in the sensitivity analysis section below.

The manufacturing cost estimates in Fig. 4 of the main text span the designs presented in Fig. 3. A breakdown of cost is also shown for a design corresponding to an electrode thickness of 100 microns and two cells connected in parallel within a series-connected cell group (i.e., voltage unit). The graphite-based Li-ion batteries used three cells connected in parallel to mitigate the larger area required due to low energy density. The design selected for the breakdown is representative of the mid-point of the projected design space examined. The items included in the subsections of the cost breakdown are detailed as follows. The purchased items include items such as cell tabs, terminals, SOC controllers, and cell and module packaging. The inactive materials subsection consists of the cost of the current collectors, electrolyte, ceramic, carbon, and binder. The pack integration components include automatic and manual disconnects that enable the safe operation of the vehicle. The non-materials contribution captures the manufacturing cost, including depreciation, labor, overhead, profit, and warranty to the cell manufacturer. The cost for energy values may be considered a price to the automaker if one ignores any markup on the pack integration components.

The inactive materials costs vary significantly across the various chemistries considered. Inactive material contributions are typically minimized by utilizing a high-voltage cell chemistry to minimize cell count and/or by utilizing a high volumetric capacity active material to decrease the area (i.e., current collector and separator) required. Increasing the volumetric capacity must occur alongside a sufficiently high electrochemical performance; otherwise, impedance and subsequent voltage losses will dictate the use of thin electrodes and thus large cell area. The major contributor to the range of cost values in the uncertainty estimate for a single chemistry is the contribution of inactive materials. Variations in the purchase price of materials, active and inactive, also contribute to the uncertainty range. Based on a previous Monte Carlo uncertainty analysis, a conservative estimation of the effect of price uncertainty for the materials and purchased items results in a contribution of -10% to the minimum cost and +20% to the maximum cost.[12]

In consideration of the active materials contribution, the lithium-metal anode contributes a significant portion to the cost of Li/O_2 batteries but a lesser amount to the Li/LMRNMC. The origin of this discrepancy is two-fold. First, less lithium is required due to the higher cell voltage of the Li/LMRNMC compared to Li/O_2. Second, the manufactured LMRNMC cathode material contains the required lithium for the cell, unlike the oxygen electrode, which initially contains no lithium. Thus, LMRNMC captures the majority of the lithium cost burden. A secondary point is that the processing cost of lithium metal per mass is higher than the LMRNMC material, reflecting the challenges of producing such a reactive metal. The lithium metal that is purchased for the Li/LMRNMC battery is only provided to meet the 50% excess buffer. While the required amount of additional lithium is uncertain, variations in the excess lithium-metal quantity will not change the relative comparison between these two cell chemistries. Comparison of the Li/LMRNMC to the Si/LMRNMC battery details the important role of lithium-metal anodes in minimizing the inactive material present in the battery.

Figures S4 and S5 present updated versions of Figs. 3 and 4 from the main text for a 50 kWh_{use} battery. The Li/O_2 open architecture system scale poorly with increasing power-to-energy ratio as the penalty for gas utilization becomes a greater portion of the total system volume, mass, and cost. The closed-system architecture scales similarly to the Li-ion based batteries. The Li/O_2 systems no longer have a mass advantage over the Li/LMRNMC and Si/LMRNMC batteries. Additionally, the energy density of the open architecture Li/O_2 system is comparable to the graphite-containing Li-ion systems. The Li/O_2 closed system continues to be projected similar in cost to the Li/LMRNMC batteries. In consideration of these estimated optimistic values, the Li/O_2 energy-storage system is not well suited for automotive applications relative to existing or more highly developed Li-ion options, particularly when the useable energy is 50 kWh or less.

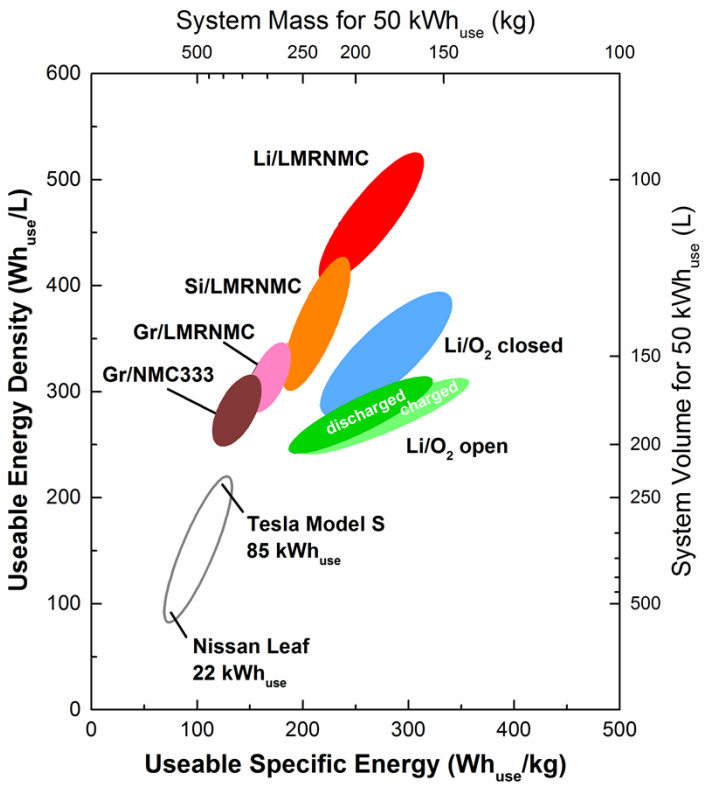

Fig. S4. Calculated systems-level energy density and specific energy for batteries with 50 kWh of useable energy and 80 kW of net power at a nominal voltage of 360 V.

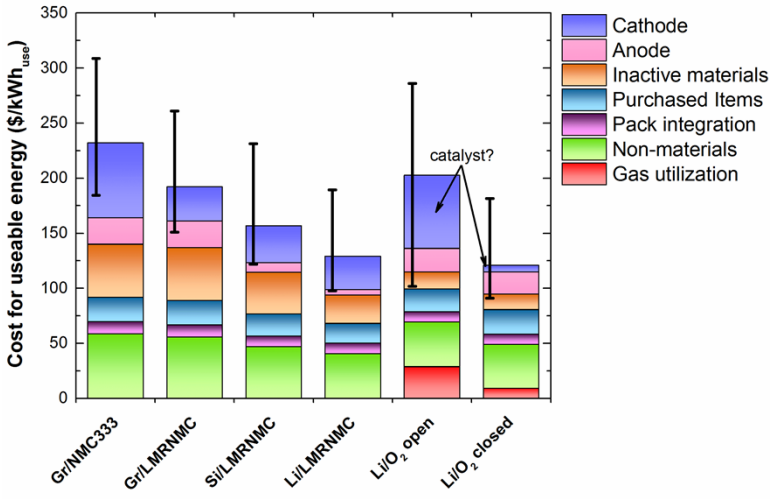

Fig. S5. Calculated systems-level cost for useable energy for batteries with 50 kWh$_{use}$ and 80 kW of net power at a nominal voltage of 360 V. Uncertainty range indicated by black bars is for the total cost for useable energy.

Li/O$_2$ open-architecture energy-storage system breakdown.

The volume and mass breakdown for a representative design of the 100 kWh$_{use}$ Li/O$_2$ open-architecture energy-storage system is shown in Fig. S6. The figure illustrates how mass and

volume are gained as function is added to enable the pack to be used and integrated into an electric vehicle. The calculated cumulative energy density and specific energy are depicted against the secondary axis. The initial drop from the theoretical maximum values results from the discharge efficiency (90%), useable SOC window (85%), and parasitic compressor energy. The energy density seems to drop precipitously with the inclusion of the excess lithium, carbon, binder, and electrolyte included in the electrode bracket. However, only a small fraction of the total system volume has been included in the energy density calculation. As seen by the mass and volume contributions, the pack and system components are the largest fractions of the battery mass and volume and are thus responsible for the largest reductions in the system energy density and specific energy. A significant mass penalty is also incurred from the copper and aluminum current collectors, as well as the ceramic solid electrolyte, which are accounted for within the bilayer. As these components are only tens of microns thick, the volume penalty for the bilayer, even though it includes the open air channels, is modest.

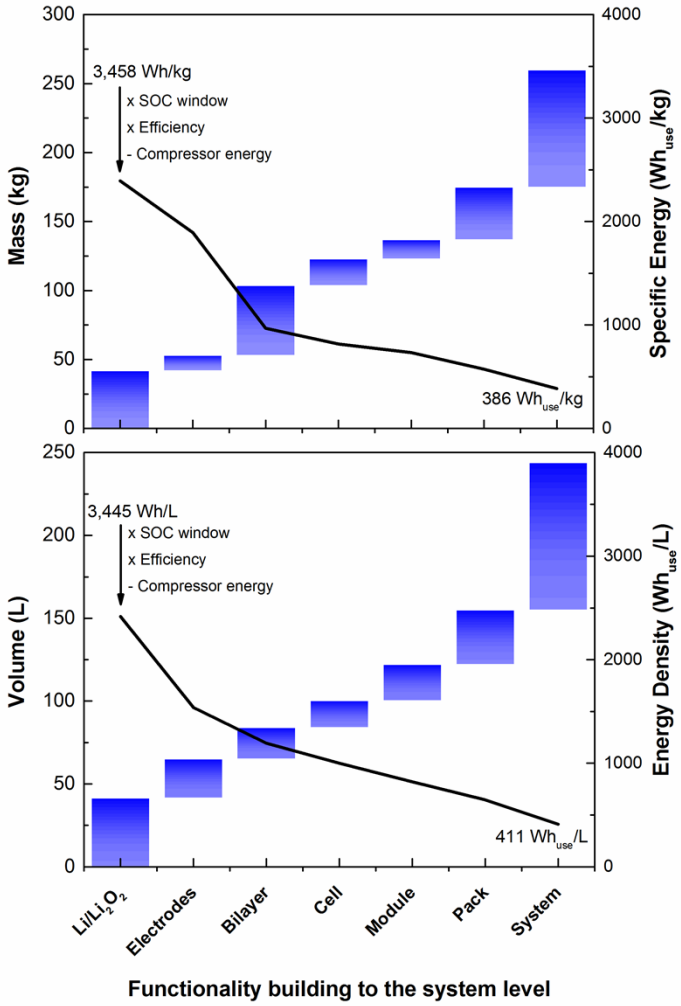

Fig. S6. Volume and mass breakdown for a Li/O_2 open-architecture energy-storage system with 100 kWh_{use} and 80 kW of net power at a nominal voltage of 360 V. Distribution of mass and volume penalties is detailed as increasing functionality is added to the active materials (from left to right). The pack bracket includes housing and insulation that surround the modules. The system bracket includes the gas utilization components necessary to deliver and purify the air.

The surprising similarity in systems-level projections between Li/O_2 and Li/LMRNMC may be understood by examining the total fraction of theoretical energy captured. Li/LMRNMC captures *ca*. 25% of theoretical while Li/O_2 reaches only *ca*. 11%, when taking into account the volumes of both the cathode and anode active materials in the theoretical baseline. The largest deviation is the inclusion of the components to compress, purify, and control or contain the gaseous reactant needed by the Li/O_2 energy-storage system. Simply put, the penalty of using gaseous oxygen as a reactant eliminates or reduces potential advantages that might have been envisioned from the theoretical specific energy and energy density.

Science and Engineering Challenges. Table 2 in the main text displays a qualitative assessment of the risk for the various chemistries and their corresponding systems reaching the projected mass, volume, and cost values in this optimistic assessment. These challenges are expanded upon in the section below if not addressed in depth in the preceding text. A concise description of the qualitative risk level used in the main text is as follows: low risk (green) is similar to batteries currently manufactured, moderate risk (yellow) has a clearly defined development path identified, although success is not guaranteed, and high risk (red) represents an extreme technical challenge with a poorly defined development path, resulting in low likelihood of achieving the projected performance and cost.

Lithium-metal anodes – The solid-electrolyte interphase (SEI) that covers the lithium surface, imparting semi-passivity, is poorly understood even after decades of research. Understanding the physicochemical and morphological basis that initiates the transport of charge, both positive and negative, through this film will lead to better understanding and control of SEIs for lithium and other SEI-forming anodes. The community has new atomic and molecular level computation, characterization, and synthetic capabilities that will allow for a fresh wave of efforts to understand this critical component of most nonaqueous batteries. Controlling the morphology of deposited lithium on both the sub-micron (i.e., dendrites) and centimeter scales (i.e., shape change) is critical to commercial implementation. Moreover, surviving the massive volume changes that come with metal electrodes will require innovative engineering and possibly new materials to mitigate the volume changes without penalizing the system-level energy density.

Lithium peroxide – The reversible and facile electrochemical conversion of the product and reactant species requires a fundamental understanding of the reaction mechanism, phase juxtaposition, and interactions of mass and charge transport in the insulating product and electrode architecture. Elucidation and control of the interaction of the peroxide species with nonaqueous electrolytes, carbon dioxide, and water are necessary to achieving the long life dictated by energy storage applications. While advances have been made in understanding the reactivity of the product Li_2O_2 with both the electrode and electrolyte, we do not see a path to the levels of performance assumed in this study.[9-11, 22, 23, 27-29] The passivation of the electrode from the insoluble discharge product is another formidable challenge.[1, 20] Overcoming this mass and charge transport balance is necessary to reach the 30 mAh/cm^2 loadings, which are also capable of 1C pulse power and C/5 discharges at 90% cell discharge efficiency.

Electrolytes – Non-volatile electrolytes are needed, perhaps in the form of solid polymers or ionic liquids, which are stable under challenging electrochemical environments while also exhibiting the necessary mass and charge transport characteristics. These electrolytes must show

stability to peroxide and superoxide intermediate species, which are the likely source of existing limitations of electrolyte stability in Li/O_2 cells. Additionally, this electrolyte must also overcome the lithium-metal challenges or have a stable interaction with an additional electrolyte that enables the lithium-metal anode.

Cell engineering – Sealing is an extremely difficult challenge that is rarely identified by the scientific community. The Li/O_2 systems must protect the lithium from the gaseous reactants that exist at much higher partial pressures than the solvent vapor. The sealing challenge is further heightened by the contraction and expansion during the charge and discharge of the lithium-metal anode. Evidence exists on a potential path forward to mitigate this challenge.[7] However, it is unknown whether this approach to sealing can meet the temperature swings, vibration exposures, and long calendar life necessitated by automotive applications. The open architecture system has the additional challenge of delivering oxygen to the flow channels that will move as the cell contracts and expands on charge and discharge. Seals will be required there as well. The closed architecture operates at high pressure, which may be a failure mechanism for the seals. The severe pressure differential will deform any gap left between the ceramic and the current collector. The corrugated flow channels will be challenging to utilize at the baseline aluminum thickness of 20 microns. It is likely that thicknesses higher than 100 microns will be necessary to maintain the corrugated shape over the life of the battery. The volume change from lithium metal will need to be buffered at the electrode, cell, or module level. The current collector welds and tab welds between cells will have to be designed to withstand the continuous stresses imposed by the volume changes.

Advanced Li-ion – The LMRNMC cathode and Si anode both pose a number of significant challenges before automotive life targets can be reached. The primary challenges for the LMRNMC cathode are a continuous lowering in the average voltage upon cycling.[30, 31] The Si electrode is troubled by side reactions that consume electrolyte and lithium, resulting in capacity fade. The low coulombic efficiency of this electrode is the result of the massive volume change of Si during lithiation.[26, 32] Substantial progress has been made by reducing the targeted capacity to *ca.* 30% of the theoretical value. The reduction in capacity occurs from the use of graphitic carbon or alloying with transition metals. Both of these materials are the subject of development and commercialization efforts by many companies.

Commercialization Path - To reach the high production volumes necessary to achieve cost competitiveness, alternative markets with higher initial cost thresholds can be beneficial toward the development of the Li/O_2 technology. For example, improved battery chemistries could be developed and be beneficial for consumer electronics. However, air-based battery systems would not be amenable to these smaller applications due to the size, complexity, and cost of the supporting air delivery system.

References:

1. J. Christensen, P. Albertus, R. S. Sanchez-Carrera, T. Lohmann, B. Kozinsky, R. Liedtke, J. Ahmed and A. Kojic, *Journal of the Electrochemical Society*, 2012, 159, R1-R30.
2. G. Girishkumar, B. McCloskey, A. C. Luntz, S. Swanson and W. Wilcke, *J Phys Chem Lett*, 2010, 1, 2193-2203.
3. D. Aurbach, E. Zinigrad, Y. Cohen and H. Teller, *Solid State Ionics*, 2002, 148, 405-416.
4. J. Dahn, "Electrically Rechargeable Metal-air Batteries Compared to Advanced Lithium-ion Batteries", Scalable Energy Storage: Beyond Lithium Ion, San Jose, CA USA, August 27, 2009.
5. M. S. Whittingham, "Beyond Lithium Ion: A Reality Check", Scalable Energy Storage: Beyond Lithium Ion V, Berkeley, CA USA June 5, 2012.
6. M. S. Whittingham, *Proceedings of the IEEE*, 2012, 100, 1518.
7. S. J. Visco, Y. S. Nimon, L. C. De Jonghe, B. D. Katz, A. Petrov. Compliant seal structures for protected active metal anodes, U.S. Patent 7,824,806 PolyPlus Battery Company, 2010.
8. S. J. Visco, Y. S. Nimon, B. D. Katz. Electrochemical device component with protected alkali metal electrode, U.S. Patent 7,858,223 PolyPlus Battery Company, 2010.
9. M. M. Ottakam Thotiyl, S. A. Freunberger, Z. Peng and P. G. Bruce, *J Am Chem Soc*, 2012, 135, 494-500.
10. M. M. Ottakam Thotiyl, S. A. Freunberger, Z. Peng, Y. Chen, Z. Liu and P. G. Bruce, *Nat Mater*, 2013.
11. Z. Q. Peng, S. A. Freunberger, Y. H. Chen and P. G. Bruce, *Science*, 2012, 337, 563-566.
12. P. Nelson, K. Gallagher, I. Bloom and D. Dees, *Modeling the Performance and Cost of Lithium-Ion Batteries for Electric Vehicles*, Chemical Sciences and Engineering Division, Argonne National Laboratory, ANL-11/32, Argonne, IL USA, 2011.
13. J. S. Newman and C. W. Tobias, *Journal of the Electrochemical Society*, 1962, 109, 1183-1191.
14. N. Munichandraiah, L. Scanlon and R. Marsh, *Journal of Power Sources*, 1998, 72, 203-210.
15. H. Gan and E. S. Takeuchi, *Journal of Power Sources*, 1996, 62, 45-50.
16. Z. Ogumi, *Electrochemistry*, 2010, 78, 319-324.
17. N. Kamaya, K. Homma, Y. Yamakawa, M. Hirayama, R. Kanno, M. Yonemura, T. Kamiyama, Y. Kato, S. Hama and K. Kawamoto, *Nat Mater*, 2011, 10, 682-686.
18. B. Wang, M. Greenblatt, S. Wang and S. Hwu, *Chemistry of Materials*, 1993, 5, 23-26.
19. R. Murugan, V. Thangadurai and W. Weppner, *Angewandte Chemie International Edition*, 2007, 46, 7778-7781.
20. V. Viswanathan, J. K. Norskov, A. Speidel, R. Scheffler, S. Gowda and A. C. Luntz, *J Phys Chem Lett*, 2013, 4, 556-560.
21. Y. C. Lu, H. A. Gasteiger and Y. Shao-Horn, *J Am Chem Soc*, 2011, 133, 19048-19051.
22. B. D. McCloskey, R. Scheffler, A. Speidel, D. S. Bethune, R. M. Shelby and A. C. Luntz, *J Am Chem Soc*, 2011, 133, 18038-18041.
23. B. D. McCloskey, R. Scheffler, A. Speidel, G. Girishkumar and A. C. Luntz, *J Phys Chem C*, 2012, 116, 23897-23905.
24. Y. C. Lu, H. A. Gasteiger, E. Crumlin, R. McGuire and Y. Shao-Horn, *Journal of the Electrochemical Society*, 2010, 157, A1016-A1025.

25. H. Voorhees, C. Sliepcevich and J. Freeman, *Industrial & Engineering Chemistry*, 1956, 48, 872-881.
26. V. Etacheri, R. Marom, R. Elazari, G. Salitra and D. Aurbach, *Energy & Environmental Science*, 2011, 4, 3243-3262.
27. S. R. Gowda, A. Brunet, G. M. Wallraff and B. D. McCloskey, *The Journal of Physical Chemistry Letters*, 2012, 4, 276-279.
28. B. D. McCloskey, D. S. Bethune, R. M. Shelby, G. Girishkumar and A. C. Luntz, *J Phys Chem Lett*, 2011, 2, 1161-1166.
29. B. D. McCloskey, A. Valery, A. C. Luntz, S. R. Gowda, G. M. Wallraff, J. M. Garcia, T. Mori and L. E. Krupp, *The Journal of Physical Chemistry Letters*, 2013, 4, 2989-2993.
30. K. G. Gallagher, J. R. Croy, M. Balasubramanian, M. Bettge, D. P. Abraham, A. K. Burrell and M. M. Thackeray, *Electrochemistry Communications*, 2013, 33, 96-98.
31. M. Sathiya, G. Rousse, K. Ramesha, C. P. Laisa, H. Vezin, M. T. Sougrati, M. L. Doublet, D. Foix, D. Gonbeau, W. Walker, A. S. Prakash, M. Ben Hassine, L. Dupont and J. M. Tarascon, *Nat Mater*, 2013, 12, 827-835.
32. U. Kasavajjula, C. Wang and A. J. Appleby, *Journal of Power Sources*, 2007, 163, 1003-1039.